

Cite this article as: Hu Jianliang, Zhao Zihan, Bo Hong, et al. Quantitative Study of Dislocation Density Evolution of 7A85 Aluminum Alloy During the Aging Treatment Process[J]. Rare Metal Materials and Engineering, 2022, 51(04): 1183-1187.

ARTICLE

Quantitative Study of Dislocation Density Evolution of 7A85 Aluminum Alloy During the Aging Treatment Process

Hu Jianliang¹, Zhao Zihan¹, Bo Hong², Jiao Ziteng¹, Jin Miao¹

¹ School of Mechanical Engineering, Yanshan University, Qinhuangdao 066012, China; ² State Key Laboratory of Metastable Materials Science and Technology, Yanshan University, Qinhuangdao 066012, China

Abstract: To reveal the dislocation evolution law of 7A85 aluminum alloy during the aging process, the influences of aging temperature and aging time on dislocation density was investigated by X-ray diffraction (XRD) and transmission electron microscopy (TEM). The results show that the dislocation density is reduced rapidly from $3.59 \times 10^{14} \text{ m}^{-2}$ to $0.62 \times 10^{14} \text{ m}^{-2}$ (decreased by 82.7%) when the aging temperature increases from 80 °C to 160 °C. Similarly, the dislocation density is decreased by 41% with the extension of aging time, and it tends to a steady value after aging treatment for 12 h. Furthermore, the TEM micrographs indicate that dislocations tend to form a low-energy dislocation cell and gradually turn into subgrain. Finally, on the basis of the results of XRD and TEM, the dislocation densities of dislocation entanglement, dislocation cell and subgrain were quantified.

Key words: dislocation density; 7A85 aluminum alloy; XRD profile analysis; microstructure evolution

7A85 aluminum alloy has been widely used in the aviation and space field due to its superior toughness, good plasticity, excellent hardenability and stress corrosion resistance^[1-3]. During the deformation and the heat treatment process, the dislocation density is not only closely related to the plastic flow behavior^[4-6], but also an important factor affecting the microstructure evolution of the material^[7,8]. In recent years, lots of research results have shown that the evolution of grains and the release of precipitation phase are directly affected by the dislocation density and morphological distribution during the heat treatment^[9-11]. Therefore, the dislocation evolution law needs to reveal to provide a theoretical basis for predicting the microstructure of the 7A85 aluminum alloy.

XRD line profile analysis has been commonly used to quantitatively analyze the dislocation density of metal materials recently^[12,13]. Takebayashi et al^[14] evaluated the dislocation densities in as-quenched and tempered martensitic steels with 0.3wt% C by XRD. Meanwhile, Pešička^[15] et al investigated the effects of heat treatment on dislocation density of tempered martensite ferritic steels using TEM and

XRD, and the yield results of both methods were in good agreement^[15]. X-ray profile measurement was also used to analyze the dislocation glide systems and distribution of deformed pure aluminum compared with the recovered state by Wang^[16], and the results were in good agreement with those obtained by other authors. The XRD line profile analysis for cold-drawn pearlitic steel wires indicated that the dislocation density increases sharply with the true strain, as reported by Yang^[17]. Therefore, the XRD line profile analysis has been developed to such an extent that microstructural details, such as crystallite size distribution, defects density and types can be extracted from XRD pattern.

In recent years, numerous reports have been published on the microstructure evolution of 7A85 aluminum alloy during the hot working process and the heat treatment process^[18,19]. However, there are few investigations on the evolution of dislocation density during the heat treatment process. Therefore, the effects of aging treatment process on the dislocation evolution of 7A85 aluminum alloy were investigated by XRD and TEM in this work.

Received date: April 25, 2021

Foundation item: Natural Science Foundation of Hebei Province (E2019203075); Top Young Talents Project of the Education Department of Hebei Province (BJ2019001); State Key Laboratory Program of High Performance Complex Manufacturing (Kfkt2017-07)

Corresponding author: Hu Jianliang, Ph. D., Associate Professor, School of Mechanical Engineering, Yanshan University, Qinhuangdao 066012, P. R. China, Tel: 0086-335-8052253, E-mail: hujianliang@ysu.edu.cn

Copyright © 2022, Northwest Institute for Nonferrous Metal Research. Published by Science Press. All rights reserved.

1 Materials and Methods

The nominal composition of 7A85 aluminum alloy is shown in Table 1. The isothermal compression tests were carried out on a Gleeble-3800 thermo mechanical simulator at the temperature of 350 °C with the strain rate of 1 s⁻¹, and the true strain was defined as 0.6. The specimens were solution treated at 470 °C for 4 h. Subsequently, the aging treatment of the specimens was carried out at 80, 100, 120, 140, 160 °C for 24 h and at 120 °C for 4, 8, 12, 16, 20, 24 h. The microstructure of specimens was observed by a JEM-2010 TEM. The XRD tests were carried out on a D/max-2500/pc X-ray diffractometer with a wavelength of 0.154 06 nm, an angle measuring range 2θ of 20°~80°, a scanning step length of 0.02°, a power loading of 200 mA at 40 kV. The XRD samples were mechanically polished and electro-polished to remove the stress layer introduced by mechanical grinding and polishing.

2 Results and Discussion

The X-ray diffraction line profile analysis was applied to evaluate the dislocation density quantitatively during the aging process. The linear shape $h(x)$ obtained through XRD experiments can be expressed mathematically by the equation as follows [20].

$$h(x) = f(x)g(x) = \int_{-\infty}^{+\infty} g(y)f(y-x)dy \quad (1)$$

where $g(x)$ is the geometric broadening profile, which is measured from the annealed Si specimen without defects; $f(x)$ is the physical broadening profile resulted from microstructure defects inside the metal; $h(x)$ and $g(x)$ are both obtained by XRD measurement.

The corresponding Fourier coefficient $A(L)$ of physical broadening profile was obtained through the method of Stocks' deconvolution [21], which can be expressed as two components as follows:

$$A(L) = A^p(L)A^s(L) \quad (2)$$

where $A^p(L)$ and $A^s(L)$ are particle coefficients and strain coefficients, respectively. According to Wang's theory [16], $A^p(L)$ and $A^s(L)$ can be expressed as below.

$$A^p(L) = \alpha - L/D_{\text{eff}} \quad (3)$$

$$A^s(L) = \exp(-2\beta_c L - \pi\beta_g^2 L^2) \quad (4)$$

where α is the Hook effect constant, L is the specific length perpendicular to the reflecting planes, D_{eff} is the average size of effective subcrystal, β_c and β_g are the Cauchy and Gaussian breadth of strain broadening profile, respectively. α , D_{eff} , β_c , β_g can be gained through Eq.(2) and Eq.(3) by nonlinear fitting. And the average dislocation density ρ can be achieved by the standard curves and procedures described in Ref.[16, 22].

The XRD patterns of 7A85 alloy at different aging temperatures is illustrated in Fig. 1. According to the above theory, the dislocation densities are obtained, as shown in

Table 1 Chemical composition of 7A85 aluminum alloy (wt%)

Zn	Mg	Cu	Fe	Si	Zr	Al
7.0~8.0	1.2~1.8	1.3~2.0	≤0.08	<0.06	0.08~0.15	Bal.

Fig. 2. It can be clearly seen that the dislocation densities evaluated by XRD line profile analysis range from $3.59 \times 10^{14} \text{ m}^{-2}$ to $0.62 \times 10^{14} \text{ m}^{-2}$. Dislocation density is continuously decreased by 82.7% with the increase of aging temperature. Essentially, the thermal activation energy of the atoms in the metal improves as the aging temperature grows, which enhances the ability of dislocation movement [23]. Thus, part of the opposite sign dislocations cancel each other out and rearrange, while part of tangled dislocations re-aggregate and then gradually transform into subgrain.

The XRD pattern at 120 °C for different aging time is shown in Fig. 3 and dislocation densities are obtained as shown in Fig.4. It can be seen that dislocation density is in the range of $2.10 \times 10^{14} \sim 3.60 \times 10^{14} \text{ m}^{-2}$. Obviously, during the aging process, dislocation density is decreased by nearly 41% with the extension of aging time. It can be clearly seen that dislocation density decreases rapidly at the early stage of aging process, whereas the dislocation density tends to be a steady value after aging treatment for 12 h. When the aging time is prolonged, the dislocation has more time to move, which promotes the rearrangement and cancellation of dislocation. In addition, with the increase of aging time, the precipitation of the second phase is promoted, which can impede the movement of dislocation.

Fig.5 is the TEM micrographs of the 7A85 aluminum alloy after aging treatment at 80, 100, 120, 140 and 160 °C for 24 h.

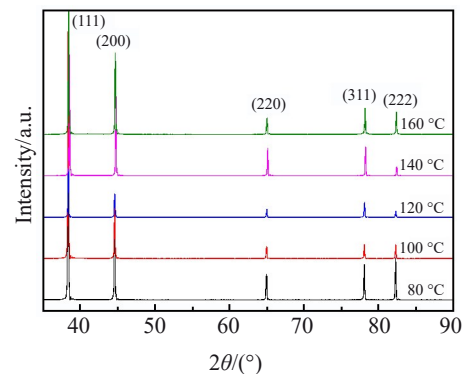


Fig. 1 XRD patterns of 7A85 aluminum alloy at different aging temperatures for 24 h

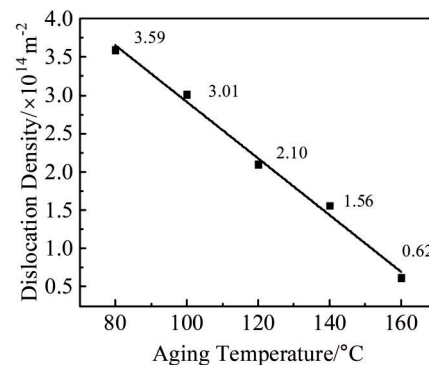


Fig. 2 Dislocation density of 7A85 aluminum alloy at different aging temperatures for 24 h

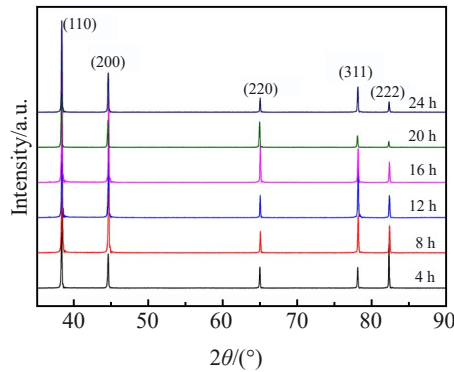


Fig.3 XRD patterns of 7A85 aluminum alloy at 120 °C with different aging time

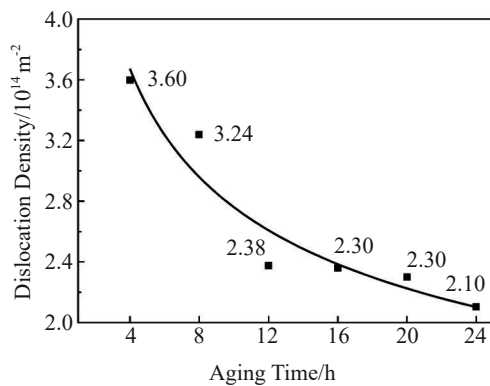


Fig.4 Dislocation density of 7A85 aluminum alloy at 120 °C for different aging time

The TEM micrographs show that dislocation climbing and cross-sliding are the important deformation modes of the 7A85 aluminum alloy with the increase of the aging

temperature. In terms of mechanism, the dislocations of opposite sign cancel each other out and rearrange^[24,25], while some of the tangled dislocations re-aggregate to substructure, as shown in Fig. 5a. With the rise of aging temperature, the motion of dislocations is enhanced. Thus, dislocations rearrange and tend to form a low-energy dislocation cell structure, as shown in Fig. 5b. As the aging process progresses, these dislocation cells will continuously absorb the dislocations around them and eventually increase the misorientation of the grain to constitute a low-angle grain boundary^[26]. At this point, a small amount of the second phase precipitates. It can be obviously observed that a small amount of dislocations are pinned by the precipitated phase in the grains, as shown in Fig. 5c. The mobility of dislocations is enhanced as the aging temperature rises to 140 °C, making it easier for dislocations to get rid of precipitates. Therefore, the dislocation density decreases, as shown in Fig. 5d. A large amount of dislocations form in the grain due to the slipping of the grain boundary, and develop into a multilateral structure. Then these multilateral structures will constantly absorb surrounding dislocations and eventually evolve into subgrain boundaries. When the aging temperature rises to 160 °C, the dislocations are greatly reduced, and a small amount of dislocations in grains are clustered together by climbing and cross-sliding movements, as shown in Fig. 5e.

Fig. 6 shows the microstructures of the 7A85 aluminum alloy at 120 °C for different aging time. It can be seen that in the whole aging process, dislocation density decreases significantly. At the initial stage of aging, there are a lot of dislocation tangling in the grains, as shown in Fig. 6a. With the extension of the aging process, dislocations have enough time to evolve and move towards the grain boundary, as seen in Fig. 6b and 6c. Besides, Fig. 6d shows that the pinning effect

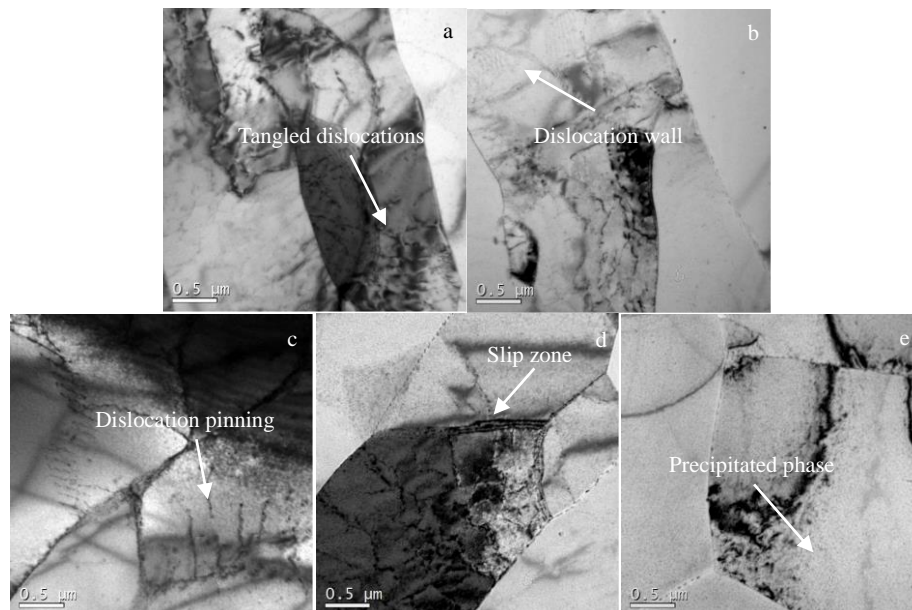


Fig.5 TEM images of 7A85 aluminum alloy at different aging temperatures for 24 h: (a) 80 °C, (b) 100 °C, (c) 120 °C, (d) 140 °C, and (e) 160 °C

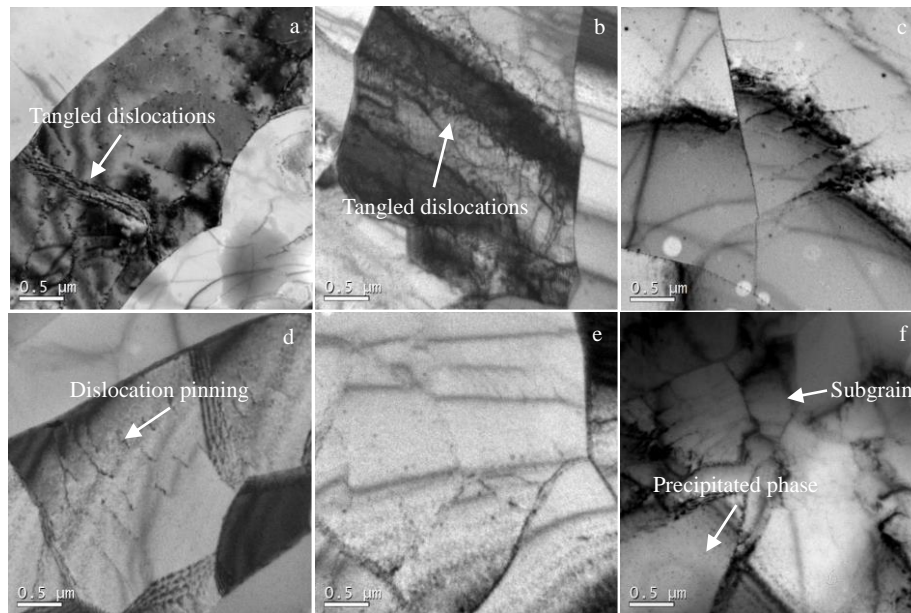


Fig.6 TEM micrographs of 7A85 aluminum alloy at 120 °C for different aging time: (a) 4 h, (b) 8 h, (c) 12 h, (d) 16 h, (e) 20 h, and (f) 24 h

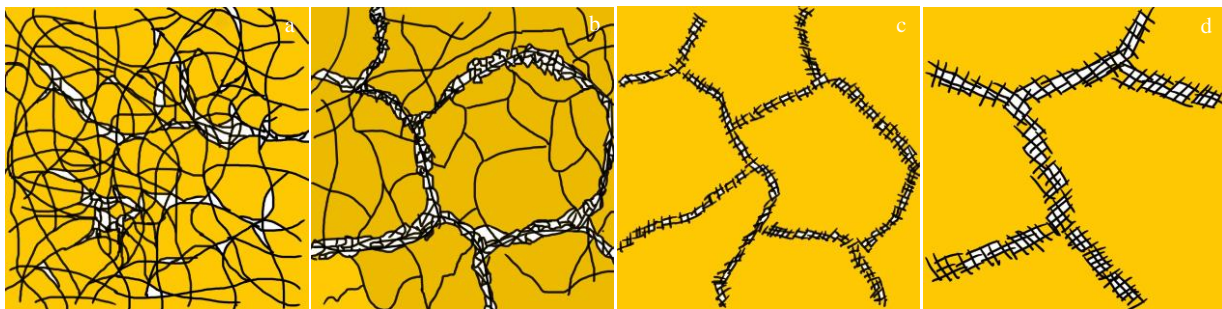


Fig.7 Dislocation evolution law of 7A85 aluminum alloy in aging process: (a) dislocation tangle, (b) dislocation cell, (c) subgrain, and (d) subgrain growth

on the dislocation movement of the precipitated phase is significant. In brief, after aging treatment, most of the dislocations are rearranged into low-energy dislocation cells and gradually turn into subgrains, as can be seen in Fig. 6e and 6f.

Consequently, the dislocation morphology of 7A85 aluminum alloy under aging process changes from dislocation entanglement to dislocation cell, and gradually turns into subgrain, as illustrated in Fig. 7. Based on XRD and TEM, the dislocation density of dislocation entanglement state is above $3.0 \times 10^{14} \text{ m}^{-2}$, as shown in Fig. 5a and 5b and Fig. 6a and 6b. As the time or the temperature increases, the dislocation cell is formed. Meanwhile, the dislocation density is reduced to around $2.0 \times 10^{14} \text{ m}^{-2}$, according to Fig. 5c and 5d and Fig. 6c~6f. Finally, the dislocation cell turns into subgrain, which has a dislocation density below $1.0 \times 10^{14} \text{ m}^{-2}$, as shown in Fig. 5e.

3 Conclusions

1) The dislocation density of 7A85 aluminum alloy in different aging treatment processes can be obtained by XRD line profile analysis. At temperature of 120 °C, with the

extension of aging time from 4 to 24 h, the dislocation density decreases, ranging from $3.6 \times 10^{14} \text{ m}^{-2}$ to $2.1 \times 10^{14} \text{ m}^{-2}$, which is decreased by 41%. As the aging temperature rises from 80 °C to 160 °C, the dislocation density is decreased by 82.7% within the range of $3.59 \times 10^{14} \text{ m}^{-2} \sim 0.62 \times 10^{14} \text{ m}^{-2}$.

2) The dislocation recovery process is remarkable with the increase of aging temperature and aging time. During the aging process, the pinning effect of dislocations on the precipitates is significant and the dislocation tends to rearrange into low-energy dislocation cell and gradually turns into subgrain, which is the main reason why the dislocation density decreases.

3) The dislocation density of dislocation entanglement, dislocation cell and subgrain is above $3.0 \times 10^{14} \text{ m}^{-2}$, around $2.0 \times 10^{14} \text{ m}^{-2}$, and below $1.0 \times 10^{14} \text{ m}^{-2}$, respectively.

References

- 1 Wen S Z, Liu C Y, Wu R L et al. *Rare Metal Materials and Engineering*[J], 2015, 44(10): 2358
- 2 Liu X G, Han S, Chen L et al. *Metallurgical and Materials*

- Transactions A*[J], 2017, 48(5): 2336
- 3 Hu J L, Yi Y P, Huang S Q. *Materials and Manufacturing Processes*[J], 2015, 30(1): 79
 - 4 Lin Y C, Nong F Q, Chen X M et al. *Vacuum*[J], 2017, 137: 104
 - 5 Thomsen S, Hopperstad O S, Myhr O R et al. *Materials Science and Engineering A*[J], 2020, 783: 139 295
 - 6 Cui F K, Ling Y F, Xue J X et al. *Chinese Journal of Mechanical Engineering*[J], 2017, 30(2): 321
 - 7 Oger L, Malard B, Odemer G et al. *Materials & Design*[J], 2019, 180: 107 901
 - 8 Zou Y, Cao L F, Wu X D et al. *Journal of Alloys and Compounds* [J], 2020, 823: 153 792
 - 9 Gurevich L M, Arisova V N, Trykov Y P et al. *Matel Science and Heat Treatment*[J], 2016, 58: 214
 - 10 Chen J F, Zou J C, Chen Y L et al. *Materials Science and Technology*[J], 2016, 32(1): 77
 - 11 Yang D L, Liu Y L, Li S B et al. *Journal of Wuhan University of Technology*[J], 2017, 32(3): 677
 - 12 Vershinina T, Leont'eva-Smirnova M. *Materials Characterization*[J], 2017, 125: 23
 - 13 Shintani T, Murata Y. *Acta Materialia*[J], 2011, 59: 4314
 - 14 Takebayashi S, Kunieda T, Yoshinaga N et al. *ISIJ International* [J], 2010, 50: 875
 - 15 Pešička J, Kužel R, Dronhofer A. *Acta Materialia*[J], 2003, 51(16): 4847
 - 16 Wang Y M, Lee S S, Lee Y C et al. *Journal of Applied Crystallography*[J], 1982, 15: 35
 - 17 Yang F, Fan Y Y, Jin Y M. *Applied Mechanics and Materials*[J], 2012, 184-185: 1054
 - 18 Yang Q Y, Liu W Y, Zhang Z Q et al. *Rare Metal Materials and Engineering*[J], 2018, 47: 409
 - 19 Yang Q Y, Deng Z H, Zhang Z Q et al. *Materials Science and Engineering A*[J], 2016, 662: 204
 - 20 Liu Y, Zhu J C, Wang Y et al. *Journal of Wuhan University of Technology*[J], 2009, 24(2): 202
 - 21 Stokes A R. *Proceedings of the Physical Society*[J], 1948, 61: 382
 - 22 Zwui S, Chen G, Wang Y M et al. *Journal of Materials Science Letters*[J], 1985, 4: 1434
 - 23 Liu W H, Qiu Q, Zhou F et al. *Rare Metal Materials and Engineering* [J], 2018, 47(1): 311 (in Chinese)
 - 24 Bai Q S, Bai J X, Hu C et al. *Materials Science and Engineering A*[J], 2018, 730: 84
 - 25 Hu S, Chen Z, Yu G G et al. *Computational Materials Science* [J], 2016, 124: 195
 - 26 Xu W F, Liu J H. *Transactions of Nonferrous Metals Society of China*[J], 2015, 25: 3212

7A85 铝合金时效处理过程中位错密度演变的定量研究

胡建良¹, 赵子寒¹, 薄 宏², 焦子腾¹, 金 淼¹

(1. 燕山大学 机械工程学院, 河北 秦皇岛 066012)

(2. 燕山大学 亚稳态材料科学与技术国家重点实验室, 河北 秦皇岛 066012)

摘 要: 采用X射线衍射 (XRD) 和透射电镜 (TEM) 研究了时效温度和时效时间对位错密度的影响, 揭示了7A85 铝合金时效过程中位错的演变规律。结果表明, 当时效温度从80 °C升高到160 °C时, 位错密度从 $3.59 \times 10^{14} \text{ m}^{-2}$ 迅速降低到 $0.62 \times 10^{14} \text{ m}^{-2}$, 降低82.7%。同样, 随着时效时间的延长, 位错密度降低了41%, 时效12 h后, 位错密度趋于稳定。TEM结果表明, 位错倾向于形成低能位错胞, 并逐渐向亚晶转变。最后, 根据XRD和TEM的结果, 分别对位错纠缠态、位错胞和亚晶粒的位错密度进行了量化。

关键词: 位错密度; 7A85 铝合金; XRD线形分析; 微观组织演变

作者简介: 胡建良, 男, 1984年生, 博士, 副教授, 燕山大学机械工程学院, 河北 秦皇岛 066012, 电话: 0335-8052253, E-mail: hujianliang@ysu.edu.cn